Role of 2-hydroxy acyl-CoA lyase HACL2 in odd-chain fatty acid production via α-oxidation in vivo

Keisuke Mori, Tatsuro Naganuma, and Akio Kihara*
Laboratory of Biochemistry, Faculty of Pharmaceutical Sciences, Hokkaido University, Sapporo 060-0812, Japan

ABSTRACT **Although most fatty acids (FAs) are even chain, certain tissues, including brain, contain relatively large quantities of odd-chain FAs in their sphingolipids. One of the pathways producing odd-chain FAs is the α-oxidation of 2-hydroxy (2-OH) FAs, where 2-OH acyl-CoA lyases (HACL1 and HACL2) catalyze the key cleavage reaction. However, the contribution of each HACL to odd-chain FA production in vivo remains unknown. Here, we found that HACL2 and HACL1 play major roles in the α-oxidation of 2-OH FAs (especially very-long-chain types) and 3-methyl FAs (other α-oxidation substrates), respectively, using ectopic expression systems of human *HACL2* and *HACL1* in yeast and analyzing *Hacl1* and/or *Hacl2* knockout (KO) CHO-K1 cells. We then generated *Hacl2* KO mice and measured the quantities of odd-chain and 2-OH lipids (free FAs and sphingolipids [ceramides, sphingomyelins, and monohexosylceramides]) in 17 tissues. We observed fewer odd-chain lipids and more 2-OH lipids in many tissues of *Hacl2* KO mice than in wild-type mice, and of these differences the reductions were most prominent for odd-chain monohexosylceramides in the brain and ceramides in the stomach. These results indicate that HACL2-involved α-oxidation of 2-OH FAs is mainly responsible for odd-chain FA production in the brain and stomach.**

Monitoring Editor
James Olzmann
University of California, Berkeley

Received: Feb 10, 2023
Revised: May 22, 2023
Accepted: May 30, 2023

INTRODUCTION

Fatty acids (FAs) are the major constituents of lipids, and most are nonhydroxylated and straight chain (not branched). In the degradation pathway, after conversion to acyl-CoAs, they are shortened by two carbons via β-oxidation, which involves oxidation at the β-position (C3). However, 2-hydroxy (2-OH) FAs with a hydroxyl group at the α-position (C2) or FAs with a methyl group at the β-position cannot undergo β-oxidation and are instead converted to FAs that are one carbon shorter through a specialized oxidation process called α-oxidation (Foulon *et al.*, 2005; Jansen and Wanders, 2006; Casteels *et al.*, 2007). The resulting odd-chain, non-hydroxy (non-OH) FAs (from 2-OH FAs) and 2-methyl FAs (from 3-methyl FAs) can be subjected to β-oxidation (Singh *et al.*, 1990; Verhoeven *et al.*, 1998; Kemp and Wanders, 2007). Although most FAs in mammals are even chain, certain tissues, such as the brain, contain relatively large quantities of odd-chain FAs, especially as components of sphingolipids (Svennerholm and Ställberg-Stenhagen, 1968). In addition to the α-oxidation of 2-OH FAs, odd-chain FAs can also be produced when the FA synthase uses propionyl-CoA as a starting material (Tove, 1959). However, the relative contributions of these two pathways to odd-chain FA production are unknown.

Phytanic acid is a well-known 3-methyl FA that is subjected to α-oxidation in humans (Jansen and Wanders, 2006; Wanders *et al.*, 2011). Phytol groups in plant chlorophyll are converted to phytanic acid by intestinal bacteria during digestion by ruminants (Hellgren, 2010; Wanders *et al.*, 2011). Humans absorb phytanic acid from their diet, especially from foods produced by grazing ruminants, and metabolize it via α-oxidation, which is carried out in four steps: CoA addition by acyl-CoA synthetases, hydroxylation at C2 by a phytanoyl-CoA 2-hydroxylase, cleavage between C1 and C2 by 2-OH acyl-CoA lyases, and oxidation by aldehyde dehydrogenases (Figure 1) (Jansen and Wanders, 2006; Casteels *et al.*, 2007; Roca-Saavedra *et al.*, 2017). Mutations in the phytanoyl-CoA 2-hydroxylase gene *PHYH* cause Refsum disease, which is accompanied by ataxia, cutaneous ichthyosis, deafness, retinitis pigmentosa, cataracts, and night blindness (Jansen *et al.*, 2004). One 2-OH acyl-CoA

This article was published online ahead of print in MBoC in Press (http://www.molbiolcell.org/cgi/doi/10.1091/mbc.E23-02-0042) on June 7, 2023.

Conflict of interest: The authors declare no financial conflicts of interest.

*Address correspondence to: Akio Kihara (kihara@pharm.hokudai.ac.jp).

Abbreviations used: AMP, *N*-(4-aminomethylphenyl) pyridinium; CER, ceramide; DKO, double knockout; ER, endoplasmic reticulum; FA, fatty acid; FFA, free fatty acid; HexCER, monohexosyl ceramide; KO, knockout; LCFA, long-chain fatty acid; LC-MS/MS, liquid chromatography coupled with tandem mass spectrometry; MRM, multiple reaction monitoring; non-OH, non-hydroxy; 2-OH, 2-hydroxy; PC, phosphatidylcholine; SM, sphingomyelin; VLCFA, very-long-chain fatty acid; WT, wild-type.

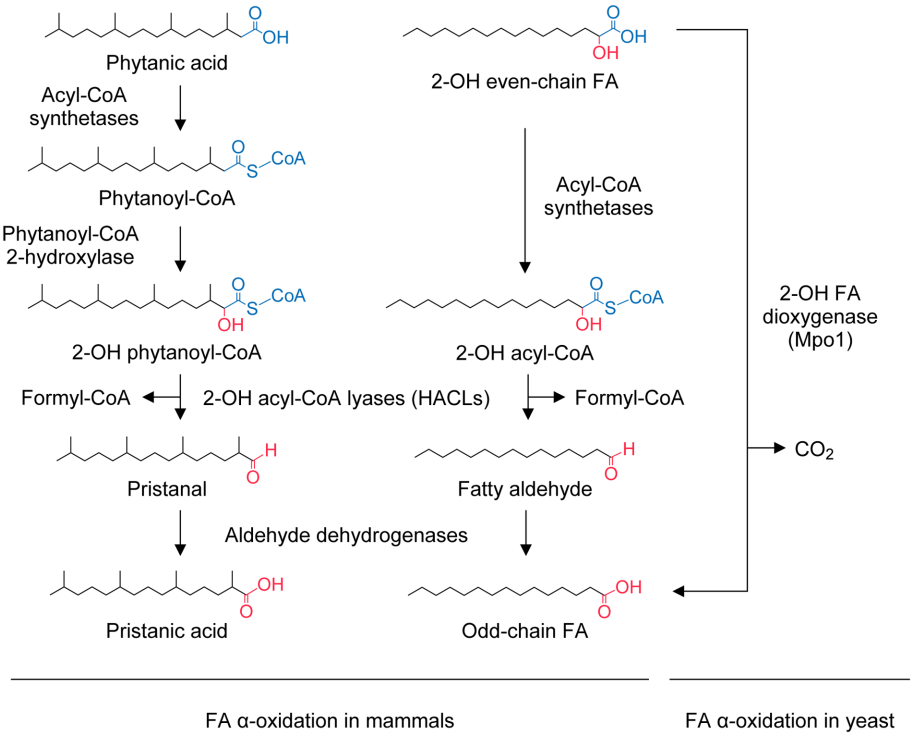

FIGURE 1: FA α-oxidation pathways in mammals and yeast. (Left) Phytanic acid (3-methyl FA) is metabolized to pristanic acid (2-methyl FA) with one fewer carbon via four reactions: CoA addition by acyl-CoA synthases, 2-hydroxylation by phytanoyl-CoA 2-hydroxylase (PHYH), cleavage between C1 and C2 by 2-OH acyl-CoA lyases (HACLs), and oxidation by aldehyde dehydrogenases. (Right) 2-OH even-chain FAs are metabolized to non-OH odd-chain FAs with one fewer carbon via three reactions in mammals (CoA addition by acyl-CoA synthases, cleavage between C1 and C2 by HACLs, and oxidation by aldehyde dehydrogenases) or one reaction catalyzed by the 2-OH FA dioxygenase Mpo1 in yeast.

lyase that is known to catalyze the third-step reaction is HACL1 (Foulon *et al.*, 1999). Although *Hacl1* knockout (KO) mice show no obvious distinct phenotype under normal growth conditions, feeding them a phytol-containing diet results in increased levels of phytanic acid in the liver and serum, loss of weight, abdominal white adipose tissue, enlargement of the liver, and reduced glycogen and triglyceride levels in the liver (Mezzar *et al.*, 2017).

2-OH FAs are present in bacteria, fungi, plants, and animals (Haak *et al.*, 1997; Ring *et al.*, 2009; Hama, 2010; Markham *et al.*, 2013; Kihara, 2016). The major membrane lipids of eukaryotes are glycerophospholipids, sphingolipids, and sterols, of which 2-OH FAs exist only in sphingolipids. Sphingolipids consist of a ceramide (CER), a hydrophobic backbone composed of a FA and a long-chain base, and a polar group, and different combinations of these constituents produce a variety of molecular species (Kihara, 2016). In mammals, the polar group is either a phosphocholine (in sphingomyelins [SMs]) or a sugar or sugar chain (in glycosphingolipids). The simplest glycosphingolipids are glucosyl CERs and galactosyl CERs, which are collectively called monohexosyl CERs (HexCERs). Sphingolipids containing 2-OH FAs have been reported to be present in specific tissues in mammals, including brain, intestines, kidney, and epidermis (Hama, 2010; Kihara, 2016). Of these, 2-OH FAs are especially abundant in the myelin of the brain as a component of galactosyl CERs, and they play an important role in maintaining myelin function and morphology (Zöller *et al.*, 2008; Dick *et al.*, 2010; Potter *et al.*, 2011). Consistent with this abundance of 2-OH FAs, their α-oxidation products—odd-chain FAs (mainly C23:0, C25:0, and C25:1)—also exist at high levels in galactosyl CERs (~20% of all HexCERs) in human brain (Svennerholm and Ställberg-Stenhagen, 1968).

2-OH FAs are produced via 2-hydroxylation of FAs by FA 2-hydroxylase or via the degradation pathway of the long-chain base phytosphingosine (Hama, 2010; Kihara, 2016; Kitamura *et al.*, 2017). The mammalian FA 2-hydroxylase is encoded by *FA2H*, whose mutations cause hereditary spastic paraplegia type 35 (SPG35) with myelin degeneration (Dick *et al.*, 2010; Rattay *et al.*, 2019). The degradation pathway of phytosphingosine with C18 produces 2-OH FA with C16:0 (Kondo *et al.*, 2014; Kitamura *et al.*, 2017). In mammals, α-oxidation of 2-OH FAs occurs via three steps (CoA addition, cleavage between C1 and C2, and oxidation; Figure 1) (Foulon *et al.*, 2005). The second step is catalyzed by 2-OH acyl-CoA lyases, which convert 2-OH acyl-CoAs to a one-carbon short fatty aldehyde and a formyl-CoA. We recently identified a novel 2-OH acyl-CoA lyase HACL2, which shares high sequence homology with HACL1 (Kitamura *et al.*, 2017). HACL1 and HACL2 show different subcellular localizations: HACL1 localizes in peroxisomes, while HACL2 is found in the endoplasmic reticulum (ER) (Foulon *et al.*, 1999; Kitamura *et al.*, 2017). HACL1 and HACL2 both function in the α-oxidation of the 2-OH C16:0 FA in the degradation pathway of phytosphingosine, with HACL2 playing the greater role (Kitamura *et al.*, 2017). In contrast, the α-oxidation of 2-OH FAs in yeast occurs in a single step and is catalyzed by 2-OH FA dioxygenase Mpo1 (Figure 1) (Kondo *et al.*, 2014; Seki *et al.*, 2019; Mori *et al.*, 2020).

FAs are classified according to chain length as long-chain FAs (LCFAs; C11–20) and very-long-chain FAs (VLCFAs; ≥C21) (Kihara, 2012). Although we have revealed that HACL2 is involved in the α-oxidation of the 2-OH LCFA (C16:0 FA) derived from phytosphingosine, it remains unclear whether it also functions in the α-oxidation of 2-OH VLCFAs, which are abundant in myelin. Further, the extent of the involvement of both HACL1 and HACL2 in the α-oxidation of 3-methyl FAs and the contribution of the α-oxidation of 2-OH FAs to the formation of odd-chain FAs in mammalian tissues are unknown. In the present study we investigated these issues using ectopic expression systems for HACL1 and HACL2 in yeast, CHO-K1 cells lacking either *Hacl1* or *Hacl2* or both, and *Hacl2* KO mice.

RESULTS

HACL2 plays a major role in the α-oxidation of straight-chain 2-OH FAs

To reveal the contributions of HACL1 and HACL2 to the α-oxidation of straight-chain 2-OH LCFAs and VLCFAs, we first performed an α-oxidation assay using an ectopic expression system in yeast. Mpo1 is the only 2-OH FA dioxygenase in yeast, and phytosphingosine-to-odd-chain FA metabolism is almost completely abolished in yeast lacking the *MPO1* gene (*mpo1*Δ) (Kondo *et al.*, 2014; Seki *et al.*, 2019). We have previously shown that expression

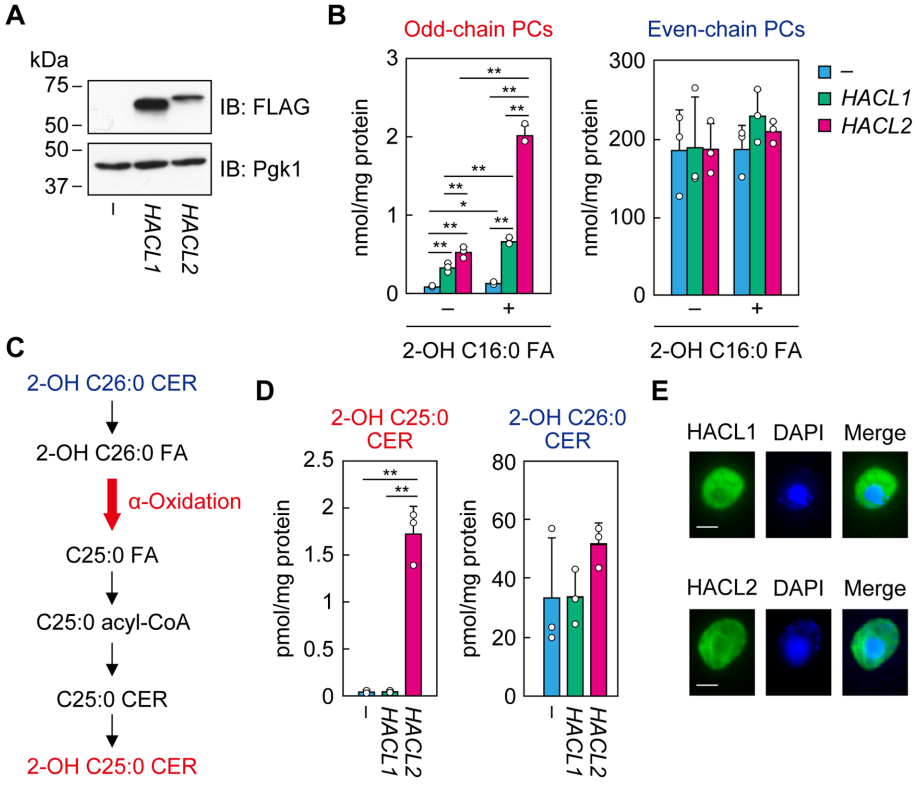

FIGURE 2: Strong contribution of HACL2 to the α-oxidation of 2-OH FAs. (A, B, D, E) Yeast strain 4378 (*mpo1*Δ) bearing the pAKNF316 (vector), pTK183 (*3 × FLAG-HACL1*), or pAKN14 (*3 × FLAG-HACL2*) plasmid was grown to log phase at 30°C. (A) Total cell lysates were prepared and separated via SDS–PAGE, followed by immunoblotting with anti-FLAG and anti-Pgk1 (for loading control) antibodies. Three independent experiments were conducted, and the result of one representative experiment is presented here. IB, immunoblotting. (B) Yeast cells were treated with 0.1% ethanol or 10 μM 2-OH C16:0 FA at 30°C for 3 h. After lipid extraction, PCs containing odd-chain (C15 and C17) FAs (left) and even-chain (C16 and C18) FAs (right) were quantified via LC-MS/MS. Values presented are means + SD ($n = 3$; * $p < 0.05$; ** $p < 0.01$; Tukey's test). (C) 2-OH C25:0 CER production pathway via α-oxidation. 2-OH C26:0 FA produced from 2-OH C26:0 CER by ceramidase is converted to C25:0 FA via α-oxidation, activated, incorporated into CER, and then hydroxylated to 2-OH C25:0 CER. (D) Lipids were extracted from yeast cells, and 2-OH C25:0 CER and 2-OH C26:0 CER were quantified via LC-MS/MS. Values presented are means + SD ($n = 3$; ** $p < 0.01$; Tukey's test). (E) Yeast cells were subjected to indirect immunofluorescence microscopy with anti-FLAG antibody. Images obtained via indirect immunofluorescence microscopy (left), by staining with 4′,6-diamidino-2-phenylindole (DAPI; middle), and by merging the two stains (right) are shown. Bars, 2 μm.

of human HACL1 or HACL2 in *mpo1*Δ cells restores this absent phytosphingosine metabolism (Kitamura *et al.*, 2017). In this study, we examined the involvement of HACL1 and HACL2 in the α-oxidation of 2-OH LCFAs and VLCFAs using *mpo1*Δ cells expressing 3 × FLAG-tagged human HACL1 or HACL2. Expression levels of HACL1 were higher than those of HACL2 (Figure 2A). The yeast cells were incubated with 2-OH C16:0 FA (a 2-OH LCFA), and we assessed the resulting quantities of phosphatidylcholines (PCs)—the most abundant glycerophospholipids in yeast—via liquid chromatography coupled with tandem mass spectrometry (LC-MS/MS). 2-OH C16:0 FA is known to be α-oxidized to C15:0 FA, converted to acyl-CoA, and then incorporated into glycerophospholipids, either directly or after FA elongation/desaturation (Kondo *et al.*, 2014; Seki *et al.*, 2019). Without the addition of 2-OH C16:0 FA, the quantities of PCs containing an odd-chain FA (odd-chain PCs) were greater in cells expressing HACL1 or HACL2 than in vector-transfected cells (4.0- and 6.4-fold greater in HACL1- and HACL2-expressing cells, respectively; Figure 2B). However, expression of HACL1 or HACL2 did not affect the quantities of PCs containing even-chain FAs, which are not metabolites in the α-oxidation pathway. Treatment with 2-OH C16:0 FA increased the levels of odd-chain PCs (2.0- and 3.9-foldin HACL1- and HACL2-expressing cells, respectively, of the levels in cells without treatment), and the quantity in HACL2-expressing cells was 3.1-fold that in HACL1-expressing cells. These results indicate that both HACL1 and HACL2 are active in the α-oxidation of 2-OH LCFAs, with HACL2 showing greater activity.

To reveal the involvement of HACL1 and HACL2 in the α-oxidation of 2-OH VLCFAs, we examined the levels of 2-OH C25:0 FA-containing CER (2-OH C25:0 CER) in *mpo1*Δ cells expressing HACL1 or HACL2. In yeast, most of the FA that constitutes CERs is 2-OH C26:0 FA (Haak *et al.*, 1997; Dickson, 2008; Ejsing *et al.*, 2009). 2-OH C26:0 CER is metabolized to 2-OH C25:0 CER via a multi-step reaction involving α-oxidation (Figure 2C). Almost no difference in 2-OH C25:0 CER levels was observed between vector-transfected and HACL1-expressing cells (Figure 2D). In contrast, 2-OH C25:0 CER levels were greatly increased by HACL2 expression (42-fold those in vector-transfected cells). The quantities of 2-OH C26 CER were comparable among vector-transfected cells, HACL1-expressing cells, and HACL2-expressing cells.

To examine the subcellular localization of HACL1 and HACL2 in yeast, we performed indirect immunofluorescence microscopy. We observed HACL1 throughout the cytosol (Figure 2E), which differs from its peroxisomal localization in mammalian cells (Foulon *et al.*, 1999; Kitamura *et al.*, 2017). Ectopic expression of HACL1 in yeast may cause the peroxisome-targeting sequence of HACL1 to be nonfunctional. Because the cytosol is in contact with the cytosolic leaflet of the ER membrane, HACL1 is involved in the α-oxidation of 2-OH LCFAs (Figure 2B). In contrast, HACL2 showed a staining pattern characteristic of the ER, that is, a double-ring structure consisting of the nuclear and peripheral ERs (Figure 2E). Thus, HACL2 seems to be localized in the ER not only in mammalian cells (Foulon *et al.*, 1999; Kitamura *et al.*, 2017) but also in yeast. It is possible that the localization of HACL1 (cytosol) and HACL2 (ER) in yeast affects the degree of their involvement in the α-oxidation of 2-OH LCFAs/VLCFAs.

Next, we examined the involvement of HACL1 and HACL2 in the α-oxidation of 2-OH VLCFAs using mammalian cells. Wild-type (WT), *Hacl1* KO, *Hacl2* KO, and *Hacl1 Hacl2* double KO (DKO) CHO-K1 cells were cultured in medium with or without 2-OH C24:0 FA for 72 h. Lipids were then extracted from the cells and subjected to CER measurements via LC-MS/MS. In the absence of 2-OH C24:0 FA, there was almost no difference in 2-OH C24:0

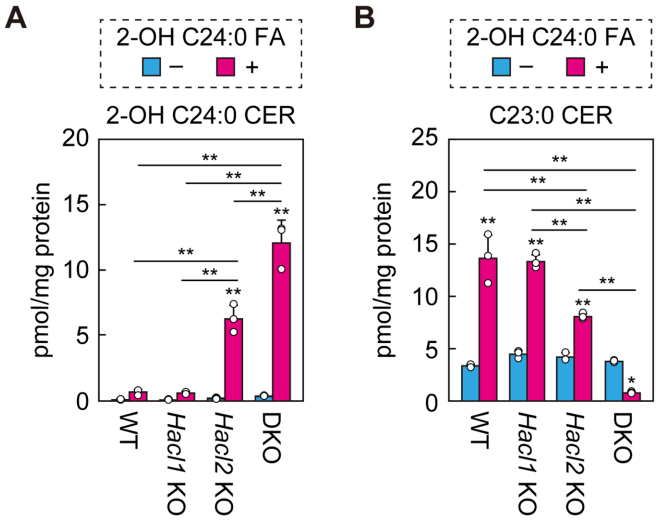

FIGURE 3: Strong contribution of HACL2 to α-oxidation of 2-OH VLCFAs. CHO-K1 (WT), *Hacl1* KO, *Hacl2* KO, and *Hacl1 Hacl2* DKO cells were incubated with 0.04% dimethyl sulfoxide (DMSO) or 4 μM 2-OH C24:0 FA for 72 h. Lipids were extracted from the cells, and 2-OH C24:0 CER (A) and C23:0 CER (B) were quantified via LC-MS/MS. Values presented are means + SD ($n = 3$; * $p < 0.05$; ** $p < 0.01$; Tukey's test).

CER levels among cell lines (Figure 3A). Treatment with 2-OH C24:0 FA increased the levels of 2-OH C24:0 CER, especially in *Hacl2* KO and DKO cells (37.4- and 34.9-fold the levels in untreated cells), and the levels were much higher than in WT cells (*Hacl2* KO cells, 9.2-fold; DKO cells, 17.8-fold). The levels of C23:0 CER, which is produced via α-oxidation of 2-OH C24:0 FA, were comparable among cell lines without 2-OH C24:0 FA addition (Figure 3B). However, addition of 2-OH C24:0 FA increased C23:0 CER levels 3–4-fold in WT and *Hacl1* KO cells and 1.9-fold in *Hacl2* KO cells but reduced them to 20% of those in untreated DKO cells. These results indicate that HACL2 plays a major role in the α-oxidation of 2-OH VLCFAs.

HACL1 plays a major role in the α-oxidation of 3-methyl branched-chain FAs

It has been shown that HACL1 is involved in the α-oxidation of phytanic acid, a 3-methyl branched-chain FA (Mezzar *et al.*, 2017), but the involvement of HACL2 was unknown. To determine this, we cultured WT, *Hacl1* KO, *Hacl2* KO, and *Hacl1 Hacl2* DKO CHO-K1 cells in medium with or without phytanic acid for 24 h. Lipids were extracted from the cells and medium, and we determined the quantities of phytanic acid and its metabolites (2-OH phytanic acid and pristanic acid; Figure 1) after alkaline treatment (to release FAs from acyl-CoAs and ester-bonded lipids). When phytanic acid was added to the medium, phytanic acid, 2-OH phytanic acid, and pristanic acid were detected in greater quantities in the medium than in the cells for all cell types (Figure 4; Supplemental Figure S1). These results indicate that the 2-OH phytanic acid and pristanic acid produced by cells are mostly released into the medium. Phytanic acid levels, both intracellular and extracellular, did not differ among cells (Figure 4A; Supplemental Figure S1A). The levels of 2-OH phytanic acid were similar in WT and *Hacl2* KO cells but higher in *Hacl1* KO cells and much higher in DKO cells (Figure 4B; Supplemental Figure S1B). In contrast, the quantities of pristanic acid—a product of HACL—were lower in *Hacl1* KO cells than in WT cells and much lower in DKO cells (Figure 4C; Supplemental Figure S1C). These results indicate that HACL1 and HACL2 function redundantly in the α-oxidation of 3-methyl FAs, with the contribution of HACL1 being greater.

Tissue distribution of 2-OH FAs

The existence of 2-OH FAs—the substrates of HACL2—has been reported for several tissues, such as brain, lung, small intestine, large intestine, kidney, uterus, and epidermis tissues (Hama, 2010; Kihara, 2016), but the full picture of their distribution in mammal tissues has remained unknown. Therefore, we first examined the quantities of 2-OH free FAs (FFAs) in 17 mouse tissues via LC-MS/MS. They were most abundant in the stomach, followed by the epidermis and lung (Figure 5). In the stomach, 2-OH FFAs accounted for 2.7% of total FFAs (non-OH FFAs + 2-OH FFAs; Supplemental Figure S2). C24:0 and C26:0 species in the stomach and C16:0 species in the epidermis and lung were the predominant 2-OH FFAs. In other tissues, only small quantities of or almost no 2-OH FFAs were detected.

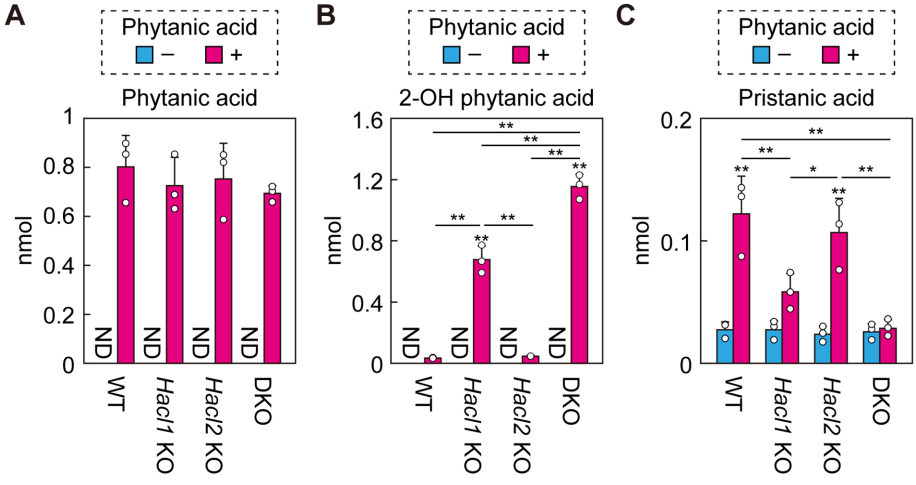

FIGURE 4: Strong contribution of HACL1 to α-oxidation of branched-chain FAs. CHO-K1 (WT), *Hacl1* KO, *Hacl2* KO, and *Hacl1 Hacl2* DKO cells were incubated with 0.04% ethanol or 4 μM phytanic acid for 24 h. Lipids were extracted from the medium and treated with alkaline, after which phytanic acid (A), 2-OH phytanic acid (B), and pristanic acid (C) were quantified via LC-MS/MS. Values presented are means + SD ($n = 3$; * $p < 0.05$; ** $p < 0.01$; Tukey's test). ND, not detected.

Because most 2-OH FAs exist in sphingolipids rather than in the free state (Hama, 2010), we then examined the quantities of 2-OH FA-containing sphingolipids (CERs, SMs, HexCERs) in 17 mouse tissues. CERs containing 2-OH FAs (2-OH CERs) were most abundant in the stomach, followed by the epidermis, submandibular glands, and bronchus (Figure 5). Only small quantities of 2-OH CERs were present in other tissues. The percentages of 2-OH CERs out of total CERs (non-OH CERs + 2-OH CERs) were ~40% in the stomach and submandibular glands and ~10% in the epidermis and bronchus (Supplemental Figure S2). The most abundant 2-OH CER species were C16:0 in the stomach, epidermis, and bronchus and C22:0 and C24:0 in the submandibular glands.

SMs are the most abundant sphingolipid class in most tissues. The submandibular

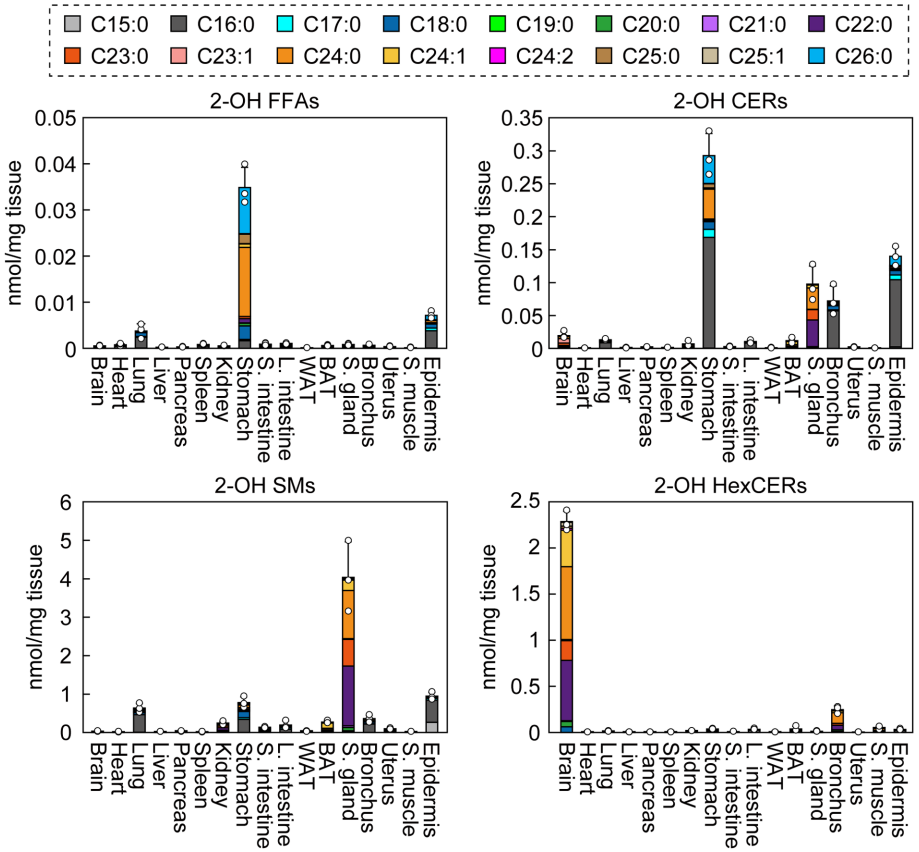

FIGURE 5: Tissue distribution of 2-OH FFAs and 2-OH sphingolipids. Lipids were extracted from 17 tissues (brain, heart, lung, liver, pancreas, spleen, kidney, stomach, small intestine, large intestine, white adipose tissue, brown adipose tissue, submandibular glands, bronchus, uterus, skeletal muscle, and epidermis) of 2-mo-old C57BL/6 mice ($n = 3$), and 2-OH FFAs, 2-OH CERs, 2-OH SMs, and 2-OH HexCERs were quantified via LC-MS/MS. Values presented are means + SD, with FA species color coded. WAT, white adipose tissue; BAT, brown adipose tissue; S. gland, submandibular gland; S. intestine, small intestine; L. intestine, large intestine; S. muscle, skeletal muscle.

glands had the highest levels of SMs containing 2-OH FAs (2-OH SMs) among the tissues examined, followed by the epidermis, stomach, and lung (Figure 5). The percentages of 2-OH SMs of total SMs (non-OH SMs + 2-OH SMs) were 41.1% in the submandibular glands, 35.0% in the epidermis, and 10.1% in the stomach (Supplemental Figure S2). In the submandibular glands, C22:0 and C24:0 species were the two most abundant 2-OH SM species (Figure 5).

The HexCERs include glucosyl CERs and galactosyl CERs, which cannot be separated by conventional LC-MS/MS. In many tissues, glucosyl CERs are the predominant HexCERs, but in the brain (myelin), galactosyl CERs are exceptionally predominant and abundant (Hama, 2010). Consistent with previous reports (Zöller *et al.*, 2008; Kanetake *et al.*, 2019), we found that 2-OH HexCERs existed at high levels in the brain but at low levels in other tissues (Figure 5). The percentage of 2-OH HexCERs of total HexCERs was 24.2% in the brain (Supplemental Figure S2). The FA composition of brain HexCERs was, in order of abundance, C24:0, C22:0, C24:1, and C23:0 (Figure 5).

Changes in the levels of 2-OH and odd-chain sphingolipids in *Hacl2* KO mice

Although we had shown that HACL2 is primarily involved in the metabolism of 2-OH FAs (Figures 2 and 3), the degree of contribution of HACL2 to the α-oxidation of 2-OH FAs and the production of odd-chain FAs in vivo remained unknown. To reveal this, we generated *Hacl2* KO mice using the CRISPR/Cas9 system and guide RNA targeting exon 7 of *Hacl2*. We obtained *Hacl2* KO mice with a 1-base-pair deletion in exon 7 (Figure 6A). The *Hacl2* KO mice grew normally, with no apparent morphological or behavioral abnormalities, and were fertile. Their body weights did not differ from those of WT mice (Figure 6B). Electron microscopy revealed no difference in myelin morphology, axon diameter, or myelin thickness between WT and *Hacl2* KO mice (Figure 6, C–E).

Lipids were extracted from 17 tissues of *Hacl2* KO mice, and the quantities of the non-OH and 2-OH types of FFAs, CERs, SMs, and HexCERs were examined via LC-MS/MS and compared with those of WT mice. Overall, the disruption of *Hacl2* increased the quantities of 2-OH species, while it reduced those of odd-chain species but left those of even-chain species unchanged or slightly increased (Figure 7; Supplemental Figures S3–S6). We then focused on the brain, stomach, and submandibular glands, which had the largest quantities of 2-OH HexCERs, 2-OH CERs, and 2-OH SMs, respectively, in WT mice (Figure 5).

In WT mouse brain, 24% of the HexCERs were 2-OH forms (Supplemental Figure S2). The primary non-OH and 2-OH HexCER species with even-chain FAs were, respectively, C24:1 species and C24:0, C22:0, and C24:1 species (Figure 8A). The quantities of some even-chain HexCER species, such as non-OH 18:0 species and 2-OH C18:0, C20:0, C24:1, and C26:0 species, were greater in *Hacl2* KO mice than in WT mice. Although the total quantities of non-OH HexCERs with even-chain FAs were similar in WT and *Hacl2* KO mouse brains, that of 2-OH HexCERs was slightly greater in *Hacl2* KO mice than in WT mice. In the WT brain, C23:1 and C23:0 species were the most abundant non-OH and 2-OH HexCER species with odd-chain FAs, respectively. In the brain of *Hacl2* KO mice, the quantities of all of the odd-chain HexCER species were reduced compared with in WT mice, and the total quantities of odd-chain HexCERs were reduced to about a quarter (non-OH HexCERs, 25.4%; 2-OH HexCERs, 28.8%) of those in WT mice, indicating that about three-quarters of the odd-chain HexCERs in the brain are produced via α-oxidation of 2-OH FAs involving HACL2. The decrease in odd-chain HexCERs caused a reduction in the total quantity (even chain + odd chain) of non-OH HexCERs in the brain of *Hacl2* KO mice (83% of that in WT mice), while that of 2-OH HexCERs was unaffected (Figure 8B). Thus, α-oxidation of 2-OH FAs involving HACL2 is important for the maintenance of non-OH HexCER levels in the mouse brain.

The major even-chain CER species in the stomach of WT mice were C24:0 and C26:0 species for non-OH CERs and C16:0, C24:0, and C26:0 species for 2-OH CERs (Figure 8C). In *Hacl2* KO mice, the quantities of many even-chain CER species were increased compared with those in WT mice, and the total quantities of non-OH

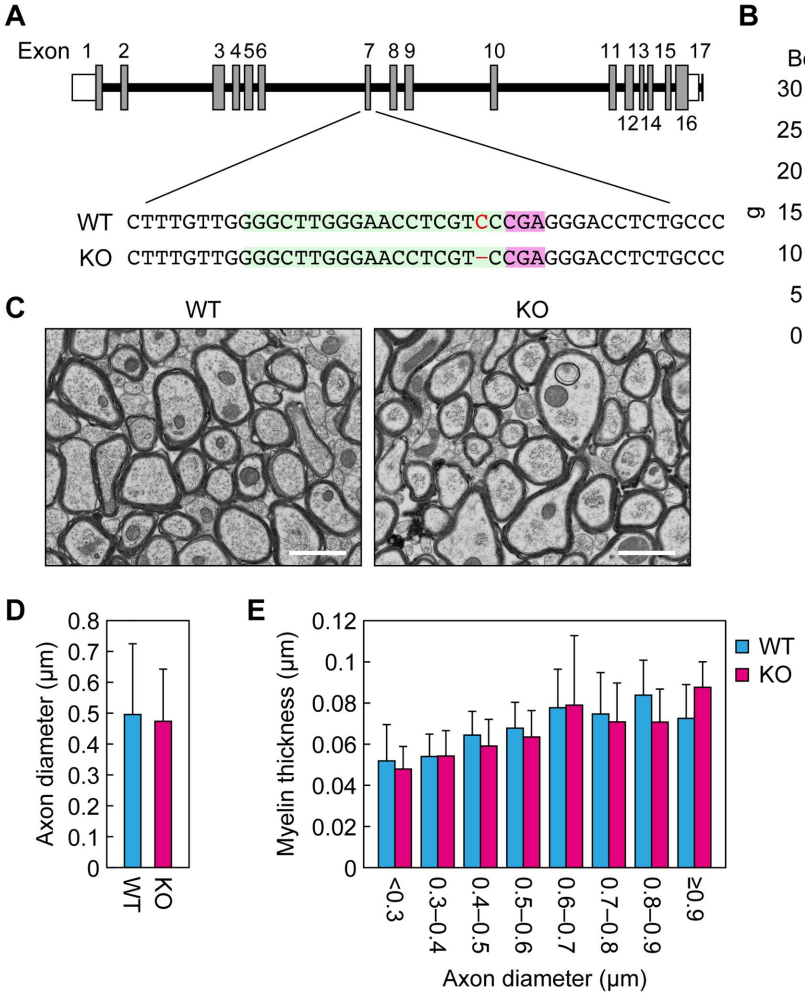

FIGURE 6: Generation of *Hacl2* KO mice and histological analysis of myelin. (A) Genome structure of the mouse *Hacl2* gene and WT and mutant nucleotide sequences around the CRISPR/Cas9 target sequence. The gray and white boxes represent coding sequences and untranslated regions, respectively. Red, deleted nucleotide in *Hacl2* KO mouse; green, target sequence of the guide RNA; pink, protospacer-adjacent motif sequence. (B) Body weights of 2-mo-old WT ($n = 12$) and *Hacl2* KO ($n = 9$) mice. Values presented are means + SD. (C–E) Transmission electron microscopy analysis of the corpus callosum in 2-mo-old WT and *Hacl2* KO mice. (C) Representative images of the sagittal sections of the corpus callosum. Scale bars, 10 μm. (D) Average diameters + SD of myelinated axons of WT ($n = 179$) and *Hacl2* KO ($n = 177$) in 12 different fields of view. (E) Myelin thickness of axons counted in D according to axon diameter. Values presented are means + SD. (B, D, E) There were no statistically significant differences between the WT and *Hacl2* KO values (two-sided Student's *t* test).

and 2-OH CERs with even-chain FAs were 1.29- and 1.48-fold those in WT mice, respectively. The most abundant odd-chain CERs in the WT mouse stomach were C25:0 species for non-OH CERs and C17:0 species for 2-OH CERs. In the stomach of *Hacl2* KO mice, the quantities of many odd-chain CER species were lower than in WT mice, and the total quantities were 53.5% (non-OH) and 38.8% (2-OH) of those in WT mice. This indicates that about half of the odd-chain CERs in the stomach are produced via α-oxidation of 2-OH FAs involving HACL2 in mice. The sums of the quantities of even- and odd-chain CERs in the stomach of *Hacl2* KO mice were 1.29-fold (not statistically significant) and 1.45-fold, respectively, of those of non-OH and 2-OH CERs in WT mice (Figure 8D).

The submandibular glands contained the highest levels of 2-OH SMs among all mouse tissues examined (Figure 5). However, unlike the brain and stomach, almost no difference was observed in the quantities of SMs between WT and *Hacl2* KO mice, regardless of whether they were non-OH or 2-OH or had odd or even chains (Supplemental Figure S7). In summary, the contribution of HACL2-involved α-oxidation of 2-OH FAs to odd-chain FA production differed among tissues, being high in the brain and stomach and low in the submandibular glands in mice.

DISCUSSION

We previously revealed that the contribution of ER-localized HACL2 to the α-oxidation of 2-OH LCFAs is greater than that of peroxisome-localized HACL1 (Kitamura *et al.*, 2017). However, their relative contributions to the α-oxidation of 3-methyl FAs and 2-OH VLCFAs remained unknown. In this study, we found that HACL1 and HACL2 contribute mainly to the α-oxidation of phytanic acid (3-methyl FA) and 2-OH VLCFAs, respectively (Figures 2–4). There are at least two possible explanations for these differential contributions. First, they could be the result of the differences in their subcellular localization: it is possible that 3-methyl FAs and 2-OH FAs are preferentially transported to peroxisomes and the ER, respectively, or the acyl-CoA synthases that convert them to acyl-CoAs may be similarly localized. The second possibility is that HACL1 and HACL2 show different substrate specificities: HACL1 may be more active toward 3-methyl acyl-CoAs and HACL2 toward 2-OH acyl-CoAs.

Because 3-methyl FAs cannot be degraded via β-oxidation, they must be excreted from the cells or converted to the β-oxidation substrate 2-methyl FAs via α-oxidation to prevent accumulation within the cells. The α-oxidation occurs via four reactions (CoA addition, 2-hydroxylation, C1–C2 cleavage, and oxidation), and the enzymes that catalyze the second (PHYH), third (HACL1), and fourth (one of the two ALDH3A2 isoforms) of these reactions are localized to peroxisomes (Mihalik *et al.*, 1997; Foulon *et al.*, 1999; Ashibe *et al.*, 2007). Because β-oxidation of 2-methyl FAs also occurs in peroxisomes (Singh *et al.*, 1990; Verhoeven *et al.*, 1998; Kemp and Wanders, 2007), the localization of the enzymes involved in α-oxidation in peroxisomes may enable the successive and efficient α- and β-oxidation of 3-methyl FAs. In contrast, straight-chain 2-OH FAs undergo α-oxidation to become odd-chain FAs with one fewer carbon, and these can be used for the biosynthesis of sphingolipids and other lipids in the ER. Therefore, α-oxidation of 2-OH FAs by HACL2 localized in the ER (Kitamura *et al.*, 2017) may be efficient for their subsequent use in lipid synthesis in the same organelle. Considering that the β-oxidation of VLCFAs occurs in peroxisomes (Kemp and Wanders, 2007), it is expected that the α-oxidation of 2-OH VLCFAs by peroxisome-localized HACL1 leads to degradation by β-oxidation rather than lipid synthesis in the ER.

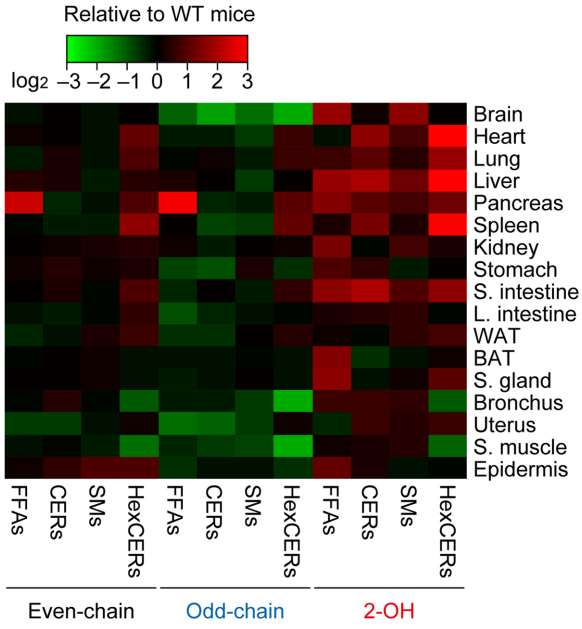

FIGURE 7: Reduced odd-chain lipids and increased 2-OH lipids in *Hacl2* KO mice. Lipids were extracted from 17 tissues (brain, heart, lung, liver, pancreas, spleen, kidney, stomach, small intestine, large intestine, white adipose tissue, brown adipose tissue, submandibular glands, bronchus, uterus, skeletal muscle, and epidermis) of 2-mo-old WT ($n = 3$) and *Hacl2* KO ($n = 3$) mice, and non-OH/2-OH FFAs, CERs, SMs, and HexCERs were quantified via LC-MS/MS. The changes in the quantities of non-OH even- and odd-chain lipids and of 2-OH lipids in *Hacl2* KO mice relative to WT mice are shown as a heat map. WAT, white adipose tissue; BAT, brown adipose tissue; S. gland, submandibular gland; S. intestine, small intestine; L. intestine, large intestine; S. muscle, skeletal muscle.

Although most FAs in mammals are even chain, relatively high percentages (5–25%) of odd-chain FAs are present in sphingolipids in some tissues (Supplemental Figures S4–S6). Odd-chain FAs can be derived from de novo FA production by FA synthase using propionyl-CoA as a precursor (Tove, 1959) or via α-oxidation of 2-OH FAs (Hajra and Radin, 1963; Kondo *et al.*, 2014), but the contribution of each pathway was until now unclear. In the present study, we found that HACL2-mediated α-oxidation contributed strongly to odd-chain FA production in the mouse brain and stomach (Figure 8). However, the contribution of HACL2 was small in other tissues, including the submandibular glands (Figure 7; Supplemental Figures S3–S7). Odd-chain FAs in these tissues may be produced via FA production from propionyl-CoA or via HACL1-mediated α-oxidation of 2-OH FAs.

In the WT mouse brain, the predominant 2-OH FAs in 2-OH HexCERs were C22:0, C24:0, and C24:1 species (Figure 8A), and their direct α-oxidation products are non-OH, odd-chain C21:0, C23:0, and C23:1 FAs. Indeed, HexCER containing C23:1 FA was the most abundant non-OH, odd-chain HexCER, while C21:0 and C23:0 species were present only at low levels. In contrast, C23:0 species were abundant among the 2-OH HexCERs. From these results we speculate that C23:0 FA produced via α-oxidation of 2-OH C24:0 FA is first 2-hydroxylated by the FA 2-hydroxylase FA2H and then metabolized to 2-OH C23:0 HexCER via 2-OH C23:0-CoA and 2-OH C23:0 CER. The high levels of 2-OH C23:0 HexCER and low levels of C23:1 species in the mouse brain suggest that the substrate specificity of FA2H is high toward saturated FAs and low toward monounsaturated FAs. It is likely that the low levels of HexCER with C21:0 FA mean that C21:0 acyl-CoA is not a good substrate for the ceramide synthase CERS2, which is abundant in the brain/myelin (Becker *et al.*, 2008), and it is therefore elongated to C23:0-CoA by FA elongase before being incorporated into CERs.

We found that 2-OH FAs are abundant in the HexCERs in the brain, CERs in the stomach, and SMs in the submandibular glands (Figure 5). The hydroxyl group present in 2-OH FAs is considered to enhance lipid–lipid interactions through hydrogen bond formation, which may enhance barrier function to prevent electrical leakage in the myelin and entry of molecules into the stomach and submandibular glands. Indeed, in the brain, 2-OH HexCERs are known to be important for myelin function and morphology (Zöller *et al.*, 2008; Dick *et al.*, 2010; Potter *et al.*, 2011). Because the stomach and submandibular glands secrete gastric acid and digestive enzymes, respectively, it is likely that they need a strong permeability barrier to protect themselves from these toxic molecules.

In the present study, we have revealed the differential contributions of HACL1 and HACL2 to the α-oxidation of 3-methyl FAs and 2-OH FAs, the in vivo contribution of HACL2 to odd-chain FA production, and the importance of HACL2-mediated α-oxidation in maintaining non-OH HexCER levels in the mouse brain. Because HACL1 and HACL2 exhibit functional redundancy, the α-oxidation pathway is not completely blocked in *Hacl2* KO mice. In the future, it is necessary to generate *Hacl1 Hacl2* DKO mice to clarify the physiological function and contribution of α-oxidation to the production of odd-chain FAs.

MATERIALS AND METHODS

Cell culture

Cells from the CHO-K1 cell line (RIKEN BioResource Research Center, Tsukuba, Japan) and their derivatives *Hacl1* KO, *Hacl2* KO, and *Hacl1 Hacl2* DKO cells (Kitamura *et al.*, 2017) were grown in Ham's F-12 medium (Merck, Darmstadt, Germany) containing 10% fetal bovine serum (Thermo Fisher Scientific, Waltham, MA), 100 U/ml penicillin, and 100 μg/ml streptomycin (Merck) at 37°C in 5% CO_2. Annual mycoplasma contamination testing confirmed that the cells used were mycoplasma-free.

Plasmids

The pAKNF316 plasmid (*URA3* marker) is a low-copy vector (*CEN* type) designed to express 3 × FLAG–tagged proteins at the N-termini under the control of the glyceraldehyde 3-phosphate dehydrogenase (*GAPDH*) promoter in yeast (Mizutani *et al.*, 2006). The pTK183 and pZKN14 plasmids are the derivatives of the pAKNF316 vector and encode 3 × FLAG–tagged human *HACL1* and *HACL2*, respectively (Kitamura *et al.*, 2017).

Yeast strains and media

Saccharomyces cerevisiae strain 4378 (*MATa his3Δ1 leu2Δ0 met15Δ0 ura3Δ0 Δmpo1::KanMX4*) was described previously (Kondo *et al.*, 2014). Cells bearing the pAKNF316, pTK183, or pZKN14 plasmid were grown in synthetic complete medium lacking uracil (0.67% yeast nitrogen base, 2% D-glucose, 0.5% casamino acids, 20 mg/l adenine, and 20 mg/l tryptophan) at 30°C.

Mice

C57BL/6J mice were purchased from Sankyo Laboratory Services (Tokyo, Japan). *Hacl2* KO mice were produced using the CRISPR/Cas9 system as follows. The guide RNA was designed to target the 20 bases adjacent to the protospacer-adjacent motif sequence

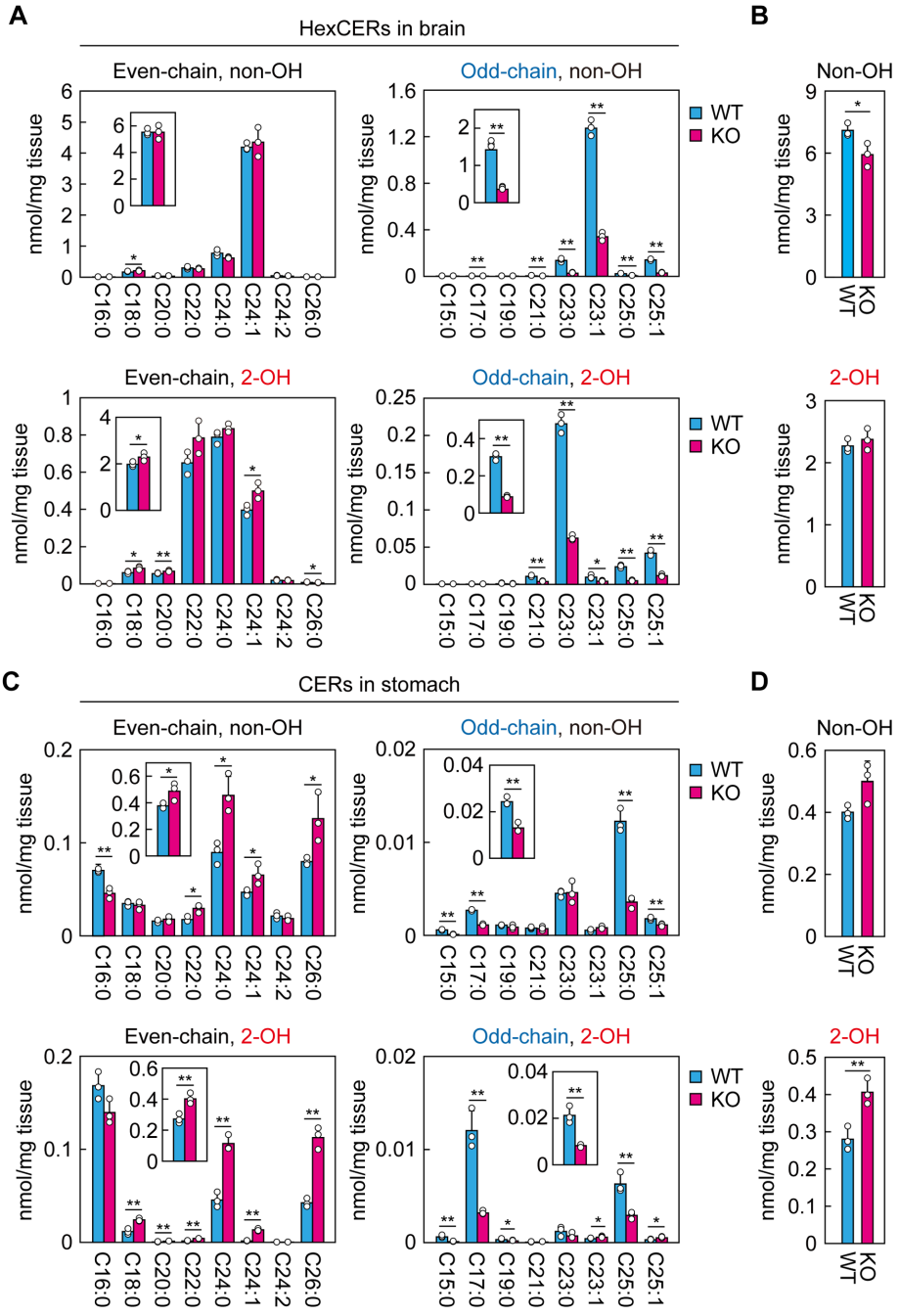

FIGURE 8: Changes in the quantities of 2-OH and odd-chain HexCERs in the brain and CERs in the stomach of *Hacl2* KO mice. Lipids were extracted from the brain (A and B) and stomach (C and D) of 2-mo-old WT and *Hacl2* KO mice, and the quantities of HexCERs (A and B) and CERs (C and D) were determined via LC-MS/MS. (A, C) Quantities of HexCER (A) and CER (C) species containing even-/odd-chain, non-OH/2-OH FAs and their total quantities (insets). (B, D) Total quantities (sum of even- and odd-chain species) of non-OH and 2-OH HexCERs (B) and CERs (D). Values presented are means + SD ($n = 3$; * $p < 0.05$; ** $p < 0.01$; two-sided Student's *t* test).

in exon 7 of *Hacl2*. The oligonucleotide pair (5′-CACCGGCTTGGGAACCTCGTCCCG-3′ and 5′-CGGGACGAGGTTCCCAAGCCGGTG-3′) containing the guide RNA sequence was annealed and cloned into the *Bbs*I site of the CRISPR/Cas9 vector pX330 (Addgene, Watertown, MA). The resulting plasmid (pKSK14) was injected into the fertilized eggs of C57BL/6J mice. We obtained a founder mouse with a 1-base-pair deletion in exon 7 of *Hacl2*. *Hacl2* KO mice were generated by crossing male and female heterozygous *Hacl2* KO mice. Mice were housed at a temperature of 23 ± 1°C, humidity of 50 ± 5%, a 12-h light/dark cycle, and free access to a standard chow diet (PicoLab Rodent Diet 20; LabDiet, St. Louis, MO) and water, under specific pathogen-free conditions. The animal experiments were approved by the institutional animal care and use committee of Hokkaido University.

Lipid analyses

Lipid extraction from yeast and LC-MS/MS measurements of odd- and even-chain PCs and CERs containing phytosphingosine were performed as described previously (Mori *et al.*, 2020). For CER measurements using cultured cells, lipids were prepared as follows. Cells grown on six-well dishes were suspended in 300 µl of lysis buffer (62.5 mM Tris-HCl [pH 6.8], 2% SDS, 10% glycerol, 5% 2-mercaptoethanol) and sonicated. A portion of the samples was used for protein quantification using the Pierce BCA Protein Assay Kit (Thermo Fisher Scientific), and another portion was used for lipid extraction. To extract lipids, samples (150 µl) were mixed with 562.5 µl of chloroform/methanol/12 M formic acid (100:200:1, vol/vol), 187.5 µl of chloroform, and 187.5 µl of water. After centrifugation (9000 × *g*, room temperature, 1 min), the organic phase containing lipids was collected, dried, suspended in methanol, diluted to appropriate concentrations, and subjected to LC-MS/MS analyses as described below.

For the measurements of phytanic acid and its metabolites from cells and medium, lipids were prepared as follows. Cell suspensions and media were mixed with a 3.75-fold volume of chloroform/methanol (1:2, vol/vol) and alkali (0.147-fold volume of 4 M KOH) and incubated at 37°C for 1 h. Samples were then neutralized with a 0.59-fold volume of 1 M HCl, mixed with a 1.25-fold volume of chloroform and a 1.25-fold volume of water, and centrifuged (9000 × *g*, room temperature, 1 min). The organic phase was collected and dried. Phytanic acid and its metabolites were derivatized with *N*-(4-aminomethylphenyl) pyridinium (AMP) amide using the AMP$^+$ Mass Spec Kit (Cayman Chemical, Ann Arbor, MI) according to the manufacturer's manual, dissolved in 1 ml of acetonitrile, and subjected to LC-MS/MS analyses as described below.

To quantify FFAs, CERs, HexCERs, and SMs in mouse tissues, tissues (bronchus, ~2 mg; others, 10–20 mg) collected from 2-mo-old mice were transferred to plastic tubes containing zirconia beads and mixed with 450 µl of chloroform/methanol/12 M formic acid

(100:200:1, vol/vol) and internal standards (100 pmol LIPIDMAPS Mass Spec Internal Standard, CER/Sphingoid Internal Standard Mix II; 50 pmol *N*-palmitoyl (d_9) D-*erythro*-sphingosine; 50 pmol *N*-(2′-(*R*)-hydroxypalmitoyl) (d_9) D-*erythro*-sphingosine; and 100 pmol d_{31}-palmitic acid, all from Avanti Polar Lipids, Alabaster, AL) vigorously (4500 rpm, 4°C, 1 min) using a Micro Smash MS-100 (TOMY Seiko, Tokyo, Japan). After centrifugation (20,400 × *g*, 4°C, 3 min), the supernatant was collected. To the pellet, 450 µl of chloroform/methanol/12 M formic acid (100:200:1, vol/vol) was added, and the lipid-extraction procedure was repeated. The collected samples were combined and mixed with 270 µl of chloroform and 486 µl of water. After centrifugation (20,400 × *g*, room temperature, 3 min), the organic phase was collected, dried, and dissolved in chloroform/methanol (1:2, vol/vol). To quantify FFAs, lipids corresponding to 1 mg of tissues (or 0.1 mg for bronchus) were dried, subjected to derivatization with AMP amide as described above, and dissolved in 1 ml of acetonitrile. For CER, SM, and HexCER measurements, 1 mg of tissues (0.1 mg for bronchus) was dried, dissolved in 375 µl of chloroform/methanol (1:2, vol/vol), and incubated with 109.7 µl of 442 mM NaOH solution at 37°C for 1 h. After neutralization with 18.9 µl of 4 M formic acid, samples were mixed with 125 µl of chloroform and 125 µl of water, followed by centrifugation (9000 × *g*, room temperature, 1 min). The organic phase was collected, dried, dissolved in chloroform/methanol (1:2, vol/vol), diluted to the appropriate concentrations, and subjected to LC-MS/MS as described below.

The LC-MS/MS analysis was performed using ultra-performance liquid chromatography with a reversed-phase column (ACQUITY UPCL CSH C18 column; particle size 1.7 µm, diameter 2.1 mm, length 100 mm; Waters, Milford, MA) and a triple quadrupole mass spectrometer (Xevo TQ-S; Waters). Lipids (injection volume, 5 µl) were ionized via electrospray ionization (capillary voltage, 3.0 kV; sampling cone, 30 V; source offset, 50 V; desolvation temperature, 500°C; desolvation gas flow, 1000 l/h; cone gas flow, 150 l/h; nebulizer gas, 7.0 bar) and detected via MS/MS in multiple reaction monitoring (MRM) mode with *m/z* values of the precursor and product ions specific for each lipid set at Q1 and Q3, respectively. PCs were detected in negative ion mode, and CERs, SMs, HexCERs, and AMP amide-derivatized FAs were detected in positive ion mode. The MRM settings for PCs and CERs were described previously (Kawana *et al.*, 2020; Mori *et al.*, 2020), whereas those for SMs, HexCERs, and AMP amide-derivatized FAs are shown in Supplemental Table S1. LC separation was performed at 55°C at a flow rate of 0.3 ml/min using a binary gradient system with mobile phase A (acetonitrile/water [3:2, vol/vol] containing 5 mM ammonium formate) and mobile phase B (acetonitrile/isopropanol [1:9, vol/vol] containing 5 mM ammonium formate). Gradient steps for PCs, CERs, SMs, and HexCERs were as follows: 0 min, 40% B; 0–18 min, gradient to 100% B; 18–23 min, 100% B; 23–23.1 min, gradient to 40% B; 23.1–25 min, 40% B. The gradient steps for AMP amide-derivatized FAs were as follows: 0 min, 10% B; 0–6 min, gradient to 40% B; 6–15 min, gradient to 70% B; 15–18 min, gradient to 100% B; 18–23 min, 100% B; 23–23.1 min, gradient to 10% B; 23.1–25 min, 10% B. The quantity of each lipid was calculated by comparing the peak area of the mass spectrogram to that of an internal or external standard. Quantification of CERs and phytanic acid and its metabolites in cultured cells and medium was performed using external standards, and that of FAs, CERs, SMs, HexCERs, and PCs in yeast cells and mouse tissues was performed using internal standards. MassLynx software (Waters) was used for data analysis.

Immunoblotting

Total cell lysates were prepared from yeast as described previously (Kihara and Igarashi, 2002). Immunoblotting was performed essentially as described previously (Kitamura *et al.*, 2015), using anti-FLAG polyclonal antibody (1:2000 dilution) (Kitamura *et al.*, 2017) and anti-Pgk1 polyclonal antibody (0.5 µg/ml) (Mori *et al.*, 2020) as the primary antibodies and horseradish peroxidase–conjugated anti-rabbit immunoglobulin G F(ab′)$_2$ fragment (1:7500 dilution; Cytiva, Marlborough, MA) as the secondary antibody. Detection was performed by immersing the protein-transferred polyvinylidene fluoride membranes in chemiluminescence reagent (100 mM Tris-HCl [pH 8.5], 0.2 mM *p*-coumaric acid, 2.5 mM luminol, 0.02% hydrogen peroxide) for 1 min and exposing them to x-ray films.

Transmission electron microscopy

Transmission electron microscopic analysis was performed using 6-mo-old mice as described previously (Isokawa *et al.*, 2019).

Indirect immunofluorescence microscopy

Indirect immunofluorescence microscopic analysis of yeast cells was performed essentially as described previously (Kihara and Igarashi, 2002). Anti-FLAG monoclonal antibody M2 (60 µg/ml; Merck) and Alexa Fluor 488–conjugated goat anti-mouse IgG (H+L) (10 µg/ml; Thermo Fisher Scientific) were used as the primary and secondary antibodies, respectively. Cells were mounted with Prolong Gold Antifade Reagent (Thermo Fisher Scientific) and observed under a Leica DM5000B microscope (Leica Microsystems, Wetzlar, Germany).

ACKNOWLEDGMENTS

We thank Takuya Kitamura and Masatoshi Miyamoto for technical support and discussion. This work was supported by Japan Society for the Promotion of Science (JSPS) KAKENHI grant number JP22H04986 (to A. K.).

REFERENCES

Ashibe B, Hirai T, Higashi K, Sekimizu K, Motojima K (2007). Dual subcellular localization in the endoplasmic reticulum and peroxisomes and a vital role in protecting against oxidative stress of fatty aldehyde dehydrogenase are achieved by alternative splicing. J Biol Chem 282, 20763–20773.

Becker I, Wang-Eckhardt L, Yaghootfam A, Gieselmann V, Eckhardt M (2008). Differential expression of (dihydro)ceramide synthases in mouse brain: oligodendrocyte-specific expression of CerS2/Lass2. Histochem Cell Biol 129, 233–241.

Casteels M, Sniekers M, Fraccascia P, Mannaerts GP, Van Veldhoven PP (2007). The role of 2-hydroxyacyl-CoA lyase, a thiamin pyrophosphate-dependent enzyme, in the peroxisomal metabolism of 3-methyl-branched fatty acids and 2-hydroxy straight-chain fatty acids. Biochem Soc Trans 35, 876–880.

Dick KJ, Eckhardt M, Paisan-Ruiz C, Alshehhi AA, Proukakis C, Sibtain NA, Maier H, Sharifi R, Patton MA, Bashir W, et al. (2010). Mutation of FA2H underlies a complicated form of hereditary spastic paraplegia (SPG35). Hum Mutat 31, E1251–E1260.

Dickson RC (2008). Thematic review series: sphingolipids. New insights into sphingolipid metabolism and function in budding yeast. J Lipid Res 49, 909–921.

Ejsing CS, Sampaio JL, Surendranath V, Duchoslav E, Ekroos K, Klemm RW, Simons K, Shevchenko A (2009). Global analysis of the yeast lipidome by quantitative shotgun mass spectrometry. Proc Natl Acad Sci USA 106, 2136–2141.

Foulon V, Antonenkov VD, Croes K, Waelkens E, Mannaerts GP, Van Veldhoven PP, Casteels M (1999). Purification, molecular cloning, and expression of 2-hydroxyphytanoyl-CoA lyase, a peroxisomal thiamine pyrophosphate-dependent enzyme that catalyzes the carbon–carbon bond cleavage during α-oxidation of 3-methyl-branched fatty acids. Proc Natl Acad Sci USA 96, 10039–10044.

Foulon V, Sniekers M, Huysmans E, Asselberghs S, Mahieu V, Mannaerts GP, Van Veldhoven PP, Casteels M (2005). Breakdown of 2-hydroxylated

straight chain fatty acids via peroxisomal 2-hydroxyphytanoyl-CoA lyase: a revised pathway for the α-oxidation of straight chain fatty acids. J Biol Chem 280, 9802–9812.
Haak D, Gable K, Beeler T, Dunn T (1997). Hydroxylation of *Saccharomyces cerevisiae* ceramides requires Sur2p and Scs7p. J Biol Chem 272, 29704–29710.
Hajra AK, Radin NS (1963). Isotopic studies of the biosynthesis of the cerebroside fatty acids in rats. J Lipid Res 4, 270–278.
Hama H (2010). Fatty acid 2-hydroxylation in mammalian sphingolipid biology. Biochim Biophys Acta 1801, 405–414.
Hellgren LI (2010). Phytanic acid—an overlooked bioactive fatty acid in dairy fat? Ann NY Acad Sci 1190, 42–49.
Isokawa M, Sassa T, Hattori S, Miyakawa T, Kihara A (2019). Reduced chain length in myelin sphingolipids and poorer motor coordination in mice deficient in the fatty acid elongase Elovl1. FASEB BioAdvances 1, 747–759.
Jansen GA, Wanders RJ (2006). Alpha-oxidation. Biochim Biophys Acta 1763, 1403–1412.
Jansen GA, Waterham HR, Wanders RJ (2004). Molecular basis of Refsum disease: sequence variations in phytanoyl-CoA hydroxylase (*PHYH*) and the PTS2 receptor (*PEX7*). Hum Mutat 23, 209–218.
Kanetake T, Sassa T, Nojiri K, Sawai M, Hattori S, Miyakawa T, Kitamura T, Kihara A (2019). Neural symptoms in a gene knockout mouse model of Sjögren-Larsson syndrome are associated with a decrease in 2-hydroxygalactosylceramide. FASEB J 33, 928–941.
Kawana M, Miyamoto M, Ohno Y, Kihara A (2020). Comparative profiling and comprehensive quantification of stratum corneum ceramides in humans and mice by LC/MS/MS. J Lipid Res 61, 884–895.
Kemp S, Wanders RJ (2007). X-linked adrenoleukodystrophy: very long-chain fatty acid metabolism, ABC half-transporters and the complicated route to treatment. Mol Genet Metab 90, 268–276.
Kihara A (2012). Very long-chain fatty acids: elongation, physiology and related disorders. J Biochem 152, 387–395.
Kihara A (2016). Synthesis and degradation pathways, functions, and pathology of ceramides and epidermal acylceramides. Prog Lipid Res 63, 50–69.
Kihara A, Igarashi Y (2002). Identification and characterization of a *Saccharomyces cerevisiae* gene, *RSB1*, involved in sphingoid long-chain base release. J Biol Chem 277, 30048–30054.
Kitamura T, Seki N, Kihara A (2017). Phytosphingosine degradation pathway includes fatty acid α-oxidation reactions in the endoplasmic reticulum. Proc Natl Acad Sci USA 114, E2616–E2623.
Kitamura T, Takagi S, Naganuma T, Kihara A (2015). Mouse aldehyde dehydrogenase ALDH3B2 is localized to lipid droplets via two C-terminal tryptophan residues and lipid modification. Biochem J 465, 79–87.
Kondo N, Ohno Y, Yamagata M, Obara T, Seki N, Kitamura T, Naganuma T, Kihara A (2014). Identification of the phytosphingosine metabolic pathway leading to odd-numbered fatty acids. Nat Commun 5, 5338.
Markham JE, Lynch DV, Napier JA, Dunn TM, Cahoon EB (2013). Plant sphingolipids: function follows form. Curr Opin Plant Biol 16, 350–357.
Mezzar S, De Schryver E, Asselberghs S, Meyhi E, Morvay PL, Baes M, Van Veldhoven PP (2017). Phytol-induced pathology in 2-hydroxyacyl-CoA lyase (HACL1) deficient mice. Evidence for a second non-HACL1-related lyase. Biochim Biophys Acta 1862, 972–990.
Mihalik SJ, Morrell JC, Kim D, Sacksteder KA, Watkins PA, Gould SJ (1997). Identification of *PAHX*, a Refsum disease gene. Nat Genet 17, 185–189.
Mizutani Y, Kihara A, Igarashi Y (2006). LASS3 (longevity assurance homologue 3) is a mainly testis-specific (dihydro)ceramide synthase with relatively broad substrate specificity. Biochem J 398, 531–538.
Mori K, Obara T, Seki N, Miyamoto M, Naganuma T, Kitamura T, Kihara A (2020). Catalytic residues, substrate specificity, and role in carbon starvation of the 2-hydroxy FA dioxygenase Mpo1 in yeast. J Lipid Res 61, 1104–1114.
Potter KA, Kern MJ, Fullbright G, Bielawski J, Scherer SS, Yum SW, Li JJ, Cheng H, Han X, Venkata JK, et al. (2011). Central nervous system dysfunction in a mouse model of FA2H deficiency. Glia 59, 1009–1021.
Rattay TW, Lindig T, Baets J, Smets K, Deconinck T, Söhn AS, Hörtnagel K, Eckstein KN, Wiethoff S, Reichbauer J, et al. (2019). FAHN/SPG35: a narrow phenotypic spectrum across disease classifications. Brain 142, 1561–1572.
Ring MW, Schwar G, Bode HB (2009). Biosynthesis of 2-hydroxy and *iso*-even fatty acids is connected to sphingolipid formation in myxobacteria. ChemBioChem 10, 2003–2010.
Roca-Saavedra P, Marino-Lorenzo P, Miranda JM, Porto-Arias JJ, Lamas A, Vazquez BI, Franco CM, Cepeda A (2017). Phytanic acid consumption and human health, risks, benefits and future trends: a review. Food Chem 221, 237–247.
Seki N, Mori K, Kitamura T, Miyamoto M, Kihara A (2019). Yeast Mpo1 is a novel dioxygenase that catalyzes the α-oxidation of a 2-hydroxy fatty acid in an Fe^{2+}-dependent manner. Mol Cell Biol 39, e00428-18.
Singh H, Usher S, Johnson D, Poulos A (1990). A comparative study of straight chain and branched chain fatty acid oxidation in skin fibroblasts from patients with peroxisomal disorders. J Lipid Res 31, 217–225.
Svennerholm L, Ställberg-Stenhagen S (1968). Changes in the fatty acid composition of cerebrosides and sulfatides of human nervous tissue with age. J Lipid Res 9, 215–225.
Tove SB (1959). Production of odd-numbered carbon fatty acids from propionate by mice. Nature 184(Suppl 21), 1647–1648.
Verhoeven NM, Roe DS, Kok RM, Wanders RJ, Jakobs C, Roe CR (1998). Phytanic acid and pristanic acid are oxidized by sequential peroxisomal and mitochondrial reactions in cultured fibroblasts. J Lipid Res 39, 66–74.
Wanders RJ, Komen J, Ferdinandusse S (2011). Phytanic acid metabolism in health and disease. Biochim Biophys Acta 1811, 498–507.
Zöller I, Meixner M, Hartmann D, Büssow H, Meyer R, Gieselmann V, Eckhardt M (2008). Absence of 2-hydroxylated sphingolipids is compatible with normal neural development but causes late-onset axon and myelin sheath degeneration. J Neurosci 28, 9741–9754.